PAPER

The Impact of Tidal Stream Turbines on Circulation and Sediment Transport in Muskeget Channel, MA

AUTHORS

Aradea R. Hakim
Geoffrey W. Cowles
School for Marine Science and Technology
University of Massachusetts, Dartmouth

James H. Churchill
Woods Hole Oceanographic Institution

ABSTRACT

The Finite-Volume Community Ocean Model (FVCOM) is configured to evaluate the potential impact of the proposed Muskeget Tidal Energy Project on circulation and sediment transport in the surrounding region. The extraction of tidal kinetic energy from the water column is modeled by augmenting the momentum equations with additional drag terms parameterized using local flow velocities and parameters specific to the installed turbine farm. Model-computed power output compares well with estimates based on velocities derived from a shipboard acoustic Doppler current profiler (ADCP). Total extracted power from the proposed installations during a spring ebb tide represents roughly 9% of the natural power in the deep section of the channel and 30% of the natural tidal dissipation in the turbine installation region. Due to this low level of extraction, turbine installations at the proposed transects result in relatively minor differences in the tidal current magnitude (2.5%), water level (0.8%), sediment flux (0.6%), and bed level (9%). Computations also indicate that the proposed installation generates minimal impacts to the tidal harmonics (3.3% change in amplitude and 1-min delay in phase) and tide-induced depth-averaged residual currents (2.8%). Model-computed extraction at increased levels is associated with greater perturbations to the natural conditions.

Keywords: tidal stream turbines, tidal energy, energy extraction, Muskeget Channel

Introduction

Muskeget Channel has been identified as a potential site for tidal energy development in the Massachusetts coastal zone (Hagerman & Bedard, 2006; Defne et al., 2012). The Town of Edgartown, Massachusetts, obtained a preliminary permit in 2008 from the Federal Energy Regulatory Commission (FERC) with the interest of developing a tidal energy project in the channel. Following an extensive observation and modeling program, the Town of Edgartown filed for a pilot license to install a 5-MW turbine array. This license is currently pending. As the technology partner for the proposed project, the Ocean Renewable Power Company (ORPC) used recently acquired velocity measurements to design a turbine array for kinetic energy extraction from the channel (McEntee, 2010).

The removal of kinetic energy from a channel flow has the potential to alter the hydrodynamics of the surrounding area (Polagye et al., 2009), changing the water circulation and the transport of sediment (James et al., 2010). In early tidal resource assessments, the potential for impact due to kinetic energy extraction was quantified using the significant impact factor (SIF), defined as the maximum ratio of extracted power to the undisturbed power that does not result in significant alterations to natural conditions. Recommended values of the SIF have ranged from 10% to 20% (Black & Veatch, 2005; ABPmer, 2007; Bryden & Couch, 2007). A recent comprehensive review of resource and impact studies for tidal energy (National Research Council, 2013) suggests that this approach be abandoned as there is no clear physical basis for the establishment of the SIF threshold. In reality, changes to the hydrodynamics and sediment transport are likely to depend on a complex variety of factors (e.g., channel bathymetry, tidal asymmetry, bed stratigraphy, turbine farm configuration), and thus, site-specific impact evaluations are necessary to accurately quantify the impact.

Impact studies using numerical models and field observation have indicated that natural levels of energy extraction by underwater turbine installations may result in maximum changes of order centimeters in water level, tens of cm/s in tidal current magnitude, and centimeters in bed

level (Neill et al., 2009, 2012). In addition, changes in residual currents (e.g., Walkington & Burrows, 2009) and Lagrangian particle excursions (e.g., Shapiro, 2011) have also been demonstrated in modeling studies. Key metrics from a field environmental monitoring program and select numerical model studies are summarized in Table 1. The field monitoring program (Royal-Haskoning, 2011) found that the 1.2 MW SeaGen Marine Current Turbine installation in Strangford Lough, consisting of a pair of 16-m diameter turbines attached to a 3-m diameter circular pile support structure resulted in a 14.5% and 7.3% change in the velocity magnitude during spring flood and ebb, respectively. During neap tide, changes in the velocity magnitude of 1.6% and 16.2% were observed during flood and ebb, respectively.

Given the large differences in findings for estimated impacts at several different proposed installations with varied levels of energy extraction (Table 1), it is clear that a site-specific study is necessary to quantify the impacts of energy extraction in Muskeget Channel with reasonable confidence. At the present stage of the proposed Muskeget Channel Tidal Energy Project, it is important to address the potential impact of proposed turbine configurations in order to move forward to commercial-scale installation while ensuring that the project is not detrimental to the environment.

The goal of this study is to investigate the influence of proposed turbine installations on circulation and sediment transport in the area surrounding Muskeget Channel. Using a hydrodynamic model, we examine the impact of tidal kinetic energy extraction on the tidally driven barotropic circulation, the residual tidal circulation, and the transport of sediment near the proposed turbine installations.

Setting

Muskeget Channel is situated to the east of Martha's Vineyard and to the west of Muskeget Island (Figure 1). It is effectively a broad open channel, roughly 700-m wide with a maximum depth of ~45 m. In 2008 and 2009, velocity data were acquired from Muskeget Channel by the Coastal Systems Program (CSP) at the School for Marine Science and Technology (SMAST) of the University of Massachusetts, Dartmouth (Howes et al., 2009). The measurements consisted of velocity profiles acquired from a shipboard acoustic Doppler current profiler (ADCP) over a full M_2 tidal cycle across transects considered for turbine installation. As revealed by the data acquired, tides within the channel are ebb-dominant. Maximum velocities observed during the ebb tide were of order 2.3 m/s. Using velocity distributions from these ADCP transects together with high-resolution channel bathymetry, ORPC designed an array of cross-flow turbines spanning four transects of the ADCP study (T6–T9 in Figure 1) (Table 2).

Methods

FVCOM

The basis of our modeling system is the Finite-Volume Community Ocean Model (FVCOM), a Fortran90 software package designed for simulation of ocean processes in coastal regions (Chen et al., 2003, 2006; Cowles, 2008). The publicly available model has a growing user base and has been used for a wide variety of applications, including storm surge modeling (Weisberg & Zheng, 2006a, 2006b) and cod larval transport (Huret et al., 2007; Churchill et al., 2011). The kernel of the code computes a solution

TABLE 1

Summary of impact magnitude of tidal energy extraction from select previous studies. The values in parentheses are the ratio of the perturbation to the natural value expressed in percent.

Authors	Power Extraction [MW] (%)	Water Level [cm] (%)	Tidal Currents [cm/s] (%)	Bed Level Change [cm](%)
Walkington and Burrows (2009)	20	2 (0.6)	22 (16)	–
Neill et al. (2009) d_{50}= 0.33 mm	250	–	-	1 (30) over 30 days
Defne et al. (2011)	11.8 (45)	5	72 (24)	–
Royal-Haskoning (2011)	1.2	–	24 (14)	–
Neill et al. (2012) d_{50}= 0.3 mm	300	–	5 (3)	0.2 (10) over 14 days
Work et al. (2013)	1.6 (60)	7	22 (16)	–

FIGURE 1

Location of the proposed turbine installation transects (T6–T9) with bathymetry contours (m) and location of the MR (Muskeget Representative) section (red) and the MIMV (Muskeget Island to Martha's Vineyard) section (blue and red). The upper subfigure on the right shows the domain of the FVCOM Massachusetts Tidal Model. The lower subfigure on the right shows the locations of the turbine in the mesh (highlighted in red). The region bordered by dashed green lines shows the area where natural tidal dissipation is evaluated. (Color versions of figures are available online at: http://www.ingentaconnect.com/content/mts/mtsj/2013/00000047/00000004.)

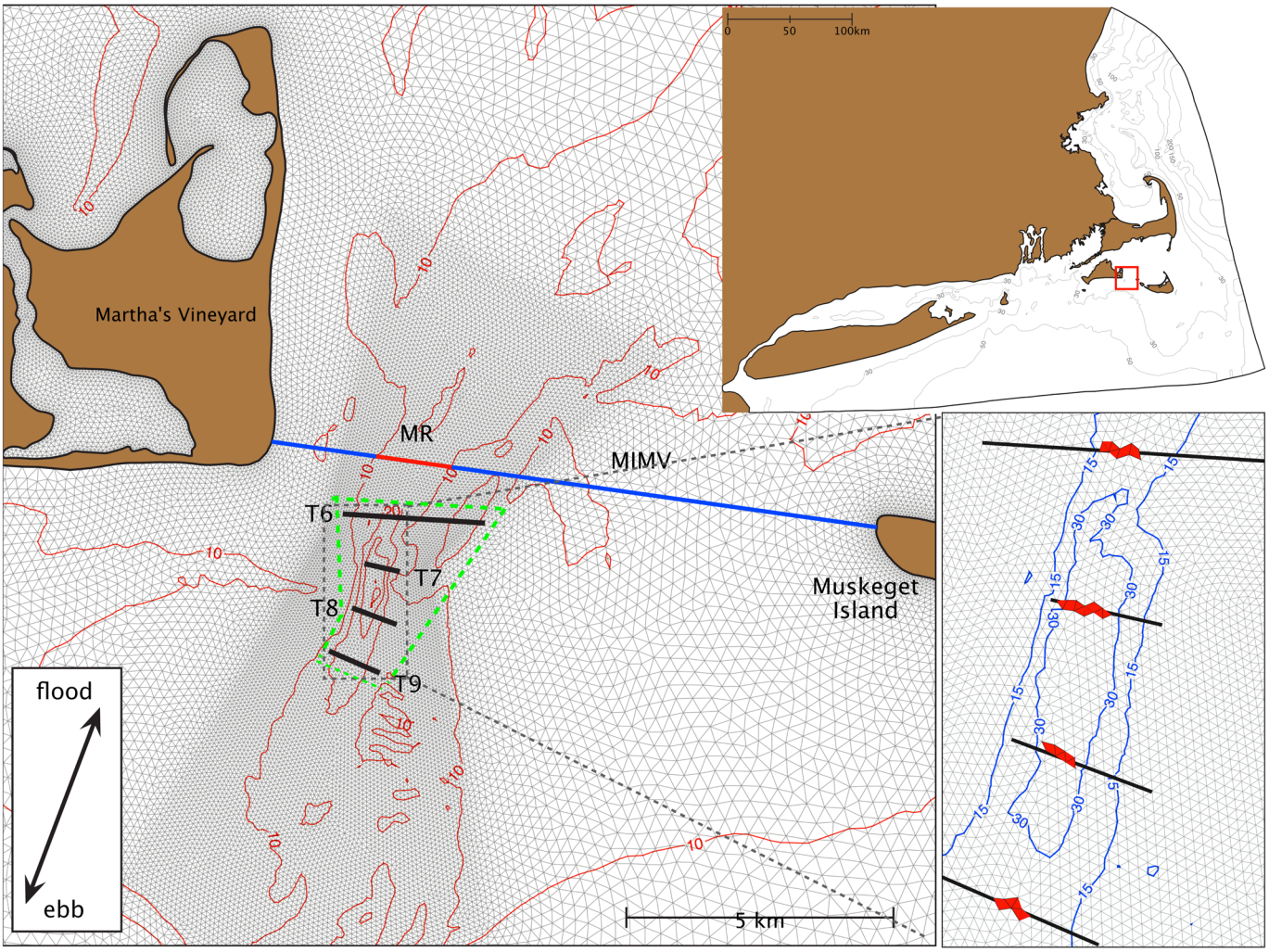

TABLE 2

Estimated turbine power output based the maximum ebb velocity measured using shipboard ADCP (McEntee, 2010).

Transect	Area[a] [m^2] A_t	Max. Vel. [m/s]	Max. Power Output [MW]
T6	1412	2.57	1.7
T7	4238	2.05	2.7
T8	2354	2.57	2.9
T9	1177	2.05	0.8

[a]Area here is the total vertical area occupied by the turbine housing and structure and is greater than the cross section of the actual turbine blades.

of the hydrostatic primitive equations on an unstructured grid using a finite-volume flux formulation with second-order spatial accuracy. The unstructured grid modeling approach is highly advantageous for resolving dynamics in regions with complex shorelines and bathymetry, such as that of Muskeget Channel and the surrounding area. For the vertical discretization, a generalized terrain-following coordinate is employed. FVCOM is interfaced to the General

Ocean Turbulence Model (GOTM) libraries (Burchard et al., 1999) to provide an array of turbulence closure schemes. We selected the k-ε model for the present work because it has demonstrated better skill in the resolution of coastal ocean processes, including buoyancy fluxes and Reynolds stresses, compared with other eddy viscosity formulations such as the Mellor-Yamada 2.5 (e.g., Ralston et al., 2010).

Marine Hydrokinetic Energy Module

For this study, we developed a Marine Hydrokinetic Energy (MHKE) module for FVCOM to simulate the effects of tidal energy extraction. In the module, the momentum equations are augmented using principles from Linear Momentum Actuator Disc Theory (Hansen, 2000; Burton, et al, 2001) to parameterize a subgrid-scale sink term (see Appendix A for a more detailed explanation). The sink term is as follows:

$$S_u = -\frac{1}{2} A_t C_x \rho u^2 \qquad (1)$$

where A_t is the cross sectional area of the turbine, C_x is the extraction coefficient (see Appendix A for derivation), ρ is the density of the fluid, and u is the magnitude of the local tidal current normal to the turbine. This momentum sink term is applied to the cells containing the turbines and is distributed uniformly in the central portion of the water column (occupying σ-layers no. 3–8 of the 10 total vertical σ-layers defined in the model). This distribution of the momentum sink terms in the column reflects the proposed position of the turbine array within the water column away from the bottom boundary layer and influence of wind-driven surface gravity waves. The model-computed turbine power output is calculated using

$$P_o = \frac{1}{2} A_t C_x \rho u^3 \qquad (2)$$

The MHKE module also accounts for augmentation of the turbulence fields due to the action of the turbines. The additional turbulence terms are parameterized following previous efforts in wind turbine modeling (Réthoré et al., 2009) and have been implemented in prior tidal turbine impact studies to eliminate the persistence wake (James et al., 2010) and to better resolve the velocity deficit and turbine wake downstream of the turbine in comparison with laboratory-scale studies (Roc et al., 2013). This approach has also been implemented by Yang et al. (2013) for idealized simulations using FVCOM. For the present work, however, we have not included the additional turbulence terms due to the uncertainty of the parameterization coefficients, and our preliminary results showed that there were no significant changes in the wake structure downstream of the turbine when employing these terms (see Appendix B for a more detailed explanation). The MHKE module was tested using an idealized open channel flow case (see Appendix C).

Sediment Transport Module

The FVCOM sediment module is based on the Community Sediment Transport Modeling System (CSTMS, Warner et al., 2008). The module includes both suspended and bedload sediment transport and simulates the mobilization, transport and settling of a number of sediment classes. For each class, parameters such as critical shear stress for erosion, median grain diameter, and settling velocity must be defined (Table 3). Properties of a user-defined number of sediment layers must also be specified. For each layer, these properties include initial (on model initiation) layer thickness, sediment class distribution, and sediment age (time since deposition). Because of sharp gradients that can occur in the near-bottom sediment concentration profile, a flux-limited scheme is used for the sediment settling equation (Jameson, 1995). The bedload transport is simulated using the MPM scheme (Meyer-Peter & Müller, 1948).

Model Setup and Execution

The simulations of our study are produced by the Massachusetts Tidal Model (MTM) (Hakim et al., in preparation), which uses FVCOM to determine barotropic tidal flows over a model domain that includes the coastal waters off of Massachusetts (Figure 1). The model grid has a mesh resolution of ~11,000 m at the open boundary decreasing to 30 m along the coast. Mesh resolution in the vicinity of Muskeget Channel is on the order of

TABLE 3

Sediment classes and properties for the sediment transport model.

Class	Grain Size (mm)	φ	w_{settle} (mm/s)	τ_{crit} (N/m^2)
Coarse sand	0.71	0.5	90.32	0.34
Very coarse sand	1.41	–0.5	142.80	0.74
Granule	2.83	–1.5	210.30	1.92
Coarse granule	5.66	–2.5	301.63	4.70

50 m. The coastal boundary of the grid is based on a high-resolution coastline developed by the Massachusetts Office of Coastal Zone Management. Grid bathymetry has been specified using a number of bathymetric data sets including: the USGS 30 arc-second Gulf of Maine database (Roworth & Signell, 1998), the NOAA 1/3 arc-second Nantucket Inundation Digital Elevation Model (covering the southern portion of Nantucket Sound; Eakins et al., 2009) and USGS Muskeget SWATH Bathymetry (encompassing the primary Muskeget Channel; Denny et al., 2012).

The model is forced by imposition of temporally changing tidal elevation at the open boundary, determined by a regional Gulf of Maine model (Chen et al., 2011). The simulations in this study are driven by six tidal constituents (M_2, S_2, N_2, K_1, O_1, and M_4) at the open boundary. The vertical coordinate is discretized into 10 layers equally spaced in the σ-coordinate. The parameterization of bottom friction requires specification of a bottom roughness (z_0). In general, z_0 is established by the grain size distribution as well as current- and wave-generated bedforms and is thus spatially and temporally variable. Given the significant complexity of resolving the true underlying roughness scales, we followed the approach of Ganju and Sherwood (2010), who investigated the influence of bottom roughness in a highly refined coupled wave-current-sediment model off the coast of Martha's Vineyard, Massachusetts, in the vicinity of Muskeget Channel. Based on their analysis, they advocated employing a constant roughness value and selected $z_0 = 0.0001$ m for their work. In this work, we used a larger value $z_0 = 0.0005$ m, which resulted in a better agreement of the tidal harmonics with observation and is reflective of the larger grain sizes found in the high-energy regions of Muskeget Channel.

Momentum is extracted, according to Equation (1), from the model cells that correspond to the turbine configuration proposed by ORPC (McEntee, 2010) (Table 2 and Figure 1). For all proposed turbine lines (Figure 1), the turbine power coefficient C_p is set to a constant value of 0.15. Note that C_p here represents the efficiency relative to the cross-sectional area of the entire installation (turbine + housing) and is thus not a reflection of the turbine efficiency, which is greater.

As noted above, a spatial distribution of sediment grain sizes must be prescribed as an initial condition to the sediment transport model. Due to the heterogeneity of the grain size distribution in the Muskeget Channel region and the paucity of grain size measurements from this region, we use the model to establish a grain size distribution that would result from tidal forcing. The procedure involves initializing a two-layer bed with equal distributions of four sediment grain sizes ranging from coarse sand (ϕ = 0.5) to coarse granule (ϕ = –2.5) in the Wentworth scale (Table 3). This multiple-layer system allows each sediment class at each specified layer to change, starting from the upper layer. Sediment at lower layer is entrained into the upper layer following erosion. The total bed thickness reflects local balances of erosion and deposition and is spatially variable. All sediments are treated as noncohesive and the larger sediments (very coarse sand to granule) are generally transported as bedload. Although larger size sediments have been observed (cobble, boulders), these are unlikely to be mobile given the shear stresses predicted by the model.

The model is executed for 60 days, at which point the grain size distribution in the bed at most model cells in the vicinity of Muskeget Channel proper has reached a quasi-steady state distribution. The resulting distribution of mean surficial grain size (Figure 2) compares well with most data points of sediment grain size extracted from the USGS usSEABED database (Poppe & Polloni, 2000) and other measurements (Howes et al., 2009). The resulting spatial distribution of fractions of the selected sediment classes is saved and used to initialize the bed in the initial sedimentation and erosion (ISE) experiments described below.

In all ISE experiments, hydrodynamic and sediment transport computations are made based on the assumption of unvarying bed topography. Because of the difficulties and computational expense associated with the simulation of bedform evolution, such an assumption is widely employed

FIGURE 2

Surficial median grain size distribution (ϕ) used to initialize the model impact experiments with USGS usSEABED (circles) and SMAST-CSP (diamonds) measurements for comparison (red = gravel, orange = gravely sediment, yellow = sand). The 15-m and 35-m isobaths are included for reference.

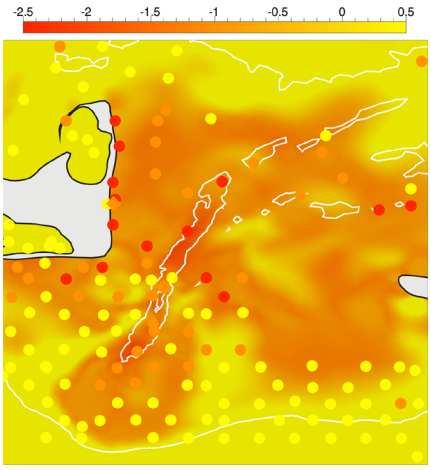

(de Vriend et al., 1993). However, because the morphodynamic feedback is not included in the ISE simulations, the results must be interpreted with caution. The net erosion/deposition predicted by the model is useful for evaluating the spatial variation of the initial adjustment of the bed to bottom stress modification resulting from the emplacement of turbines. However, interaction of the changing bathymetry with the flow field makes these predictions of bed level adjustment unreliable in the long term.

Results and Discussion

The results discussed here can be divided into two general categories based on the scale of impact: single-transect and full installation. In single-transect extraction scenarios, turbines are included along specific transects (T6–T9) using configurations outlined by ORPC. These single-transect experiments focus on effects at the scale of the tidal power installation. The properties that are considered for this scale of impact investigation are sea surface height (water level), instantaneous velocities, bed stress, sediment flux, and bed level change. The second set of experiments considers full project installation, with turbines placed along all four transects. These full-installation experiments are focused on the examination of larger-scale regional impacts, in particular, on tidal amplitude and phase, and depth-averaged residual circulation.

Turbine Power Output and Evaluation

The power output along a particular transect, calculated from the model results, agrees well with ORPC estimated power with the exception of transect T6, where the model calculation is ~40% lower than the estimated value. Close agreement of the ORPC estimated power output and the model prediction may not necessarily be expected, as the power estimates made by ORPC were based on extrapolation from a single representative velocity along a transect, rounded to the nearest knot. For the purpose of this analysis, we use the term natural power to refer to the flux of kinetic energy through a particular section without the presence of turbines.

Compared to the natural power across each transect, the maximum power extracted by the turbines according to the proposed configuration is ~6%. The time series of power extraction at each transect considered for turbine installation is shown in Figure 3 together with the natural power across a representative Muskeget section (MR, red line in Figure 1) and a Muskeget Island to Martha's Vineyard section (MIMV, blue and red line in Figure 1). The total power extracted by the proposed configuration of turbines (sum of extraction over T6, T7, T8, and T9) during peak ebb represents ~9% of the natural power along the MR section and ~3% of the natural power along the longer MIMV section.

As an additional evaluation, we compare the extracted power to the natural tidal dissipation in the region bordered by of all four transects (T6–T9). The natural tidal dissipation (Figure 3, middle panel) is estimated using the bottom stress τ_b and tidal velocity

FIGURE 3

Plots of power evaluation over a tidal cycle. Top panel: plot of model-computed extracted power at proposed transects over a tidal cycle with peak power extraction estimated from shipboard ADCP (asterisks) shown for reference. Middle panel: plot of model-computed natural power through the MIMV and MR sections and natural tidal dissipation due to bottom friction in the proposed installation region. Bottom panel: ratio of the sum of individual power extracted by the turbines to the natural power and natural tidal dissipation due to bottom friction.

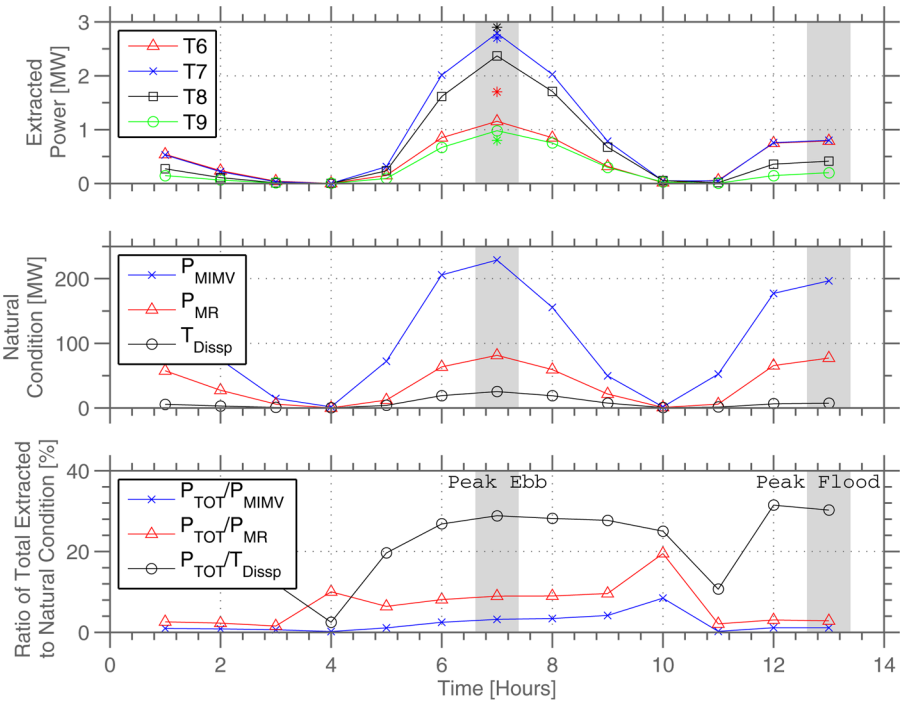

at the bottom u_b (e.g., Simpson and Hunter, 1974) integrated over the region of interest (dashed green box in Figure 1) computed with

$$T_{dissp} = \iint u_b \tau_b dA. \quad (3)$$

The maximum power extracted at each transect according to the proposed configuration is ~11% compare with the natural tidal dissipation. The total power extracted by the proposed configuration of turbines (sum of extraction over T6, T7, T8, and T9) represents 28% and 30% of natural tidal dissipation in the region during peak ebb and flood, respectively (see Figure 3, bottom panel).

Water Level

In the vicinity of Muskeget Channel proper, as defined by the region bounded by the 15-m isobath, the change in sea surface height induced by the installations is roughly 3 mm (not shown). This change is associated with a head that builds up against the device and relaxes downstream. This adverse pressure gradient is responsible for the relative decrease in velocity upstream of the turbine (Figure 4) discussed in the next section.

Instantaneous Velocity

The extraction of momentum by the turbines modifies the velocity field in the region surrounding the turbine. A momentum deficit forms in the wake and extends downstream. During ebb, the maximum velocity defect associated with energy extraction is roughly 5 cm/s (Figure 4, left panel). The velocity magnitude is also reduced upstream of the turbine, but the magnitude of the impact is less than 1 cm/s. In association with the decreased velocities and reduction of momentum is a lateral pressure gradient, which drives the flow around the turbine. This produces a velocity increase on the flanks of the channel of roughly 2 cm/s. The modification to the depth-averaged flow during flood (Figure 4, right panel) is spatially similar, but with reduced magnitude as the channel is strongly ebb-dominant.

FIGURE 4

Difference between T8 installation-modified and natural depth-averaged velocity magnitude (m/s) during ebb (a) and flood (b).

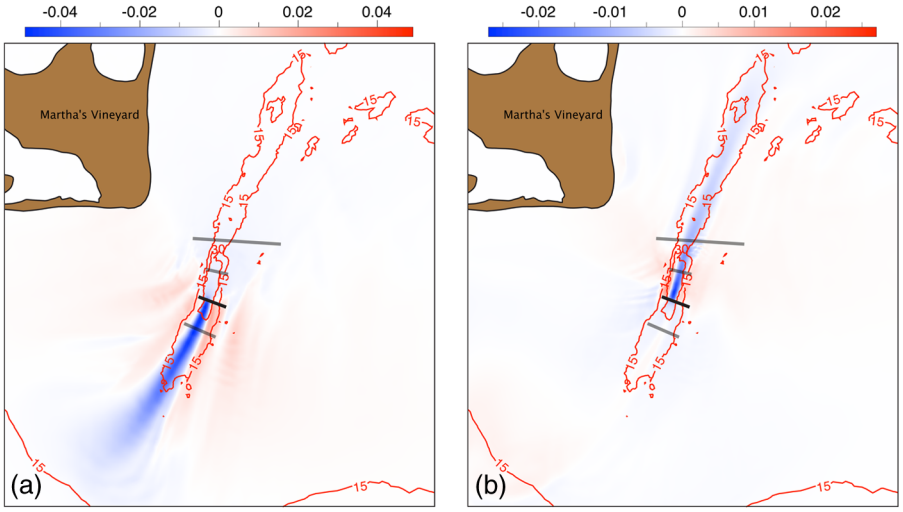

Associated with the modifications to the velocity field are perturbations to the bed stress which generally scales as the square of the velocity. During ebb, the model-computed bed stress for an installation at T8 is decreased in the main channel by ~0.25 N and increased along the flanks of the channel by ~0.1 N. On flood tide, a similar pattern appears, but the magnitude of bed stress perturbations is reduced accordingly. The spatial distribution of bed stress perturbations for installations at other transects follows the same general pattern with reduced stresses in the channel and enhanced stresses along the edges. In sediment transport simulations, it is the perturbations of current-induced bed stresses that are responsible for the changes in sediment mobilization and settling associated with the turbine emplacement.

Sediment Flux and Bed Level Change

The sediment transport experiments were initialized using a spatial distribution of sediment fractions with the median grain size shown in Figure 2. The bed was then allowed to evolve based on net deposition and erosion of the select sediment classes for 30 days under tidal forcing both with and without turbines.

Fluxes of sediment through the channel were examined along 3 transects (red lines in Figure 5a and 5b): one north and one south of the proposed area of energy extraction, and one intersecting this area (between transects T7 and T8). During ebb (Figure 5a), the model-computed, vertically integrated, natural sediment fluxes are on the order of 1 kg/(m-s) at the central and northern transects. Weaker fluxes are observed along the southern transect, indicating a divergence of sediment along the channel. During flood, fluxes are approximately 30% lower.

The effect of energy extraction can be evaluated by subtracting the instantaneous sediment fluxes computed with the subgrid-scale turbine model in place

FIGURE 5

(a) Natural sediment fluxes (suspended- and bed-load) across three transects (red lines) during ebb. (b) Difference between T7 installation-modified and natural sediment fluxes (suspended- and bed-load) across the three transects during ebb. (c) Difference between T7 installation-modified and natural bed level change [m] over a 30-day simulation.

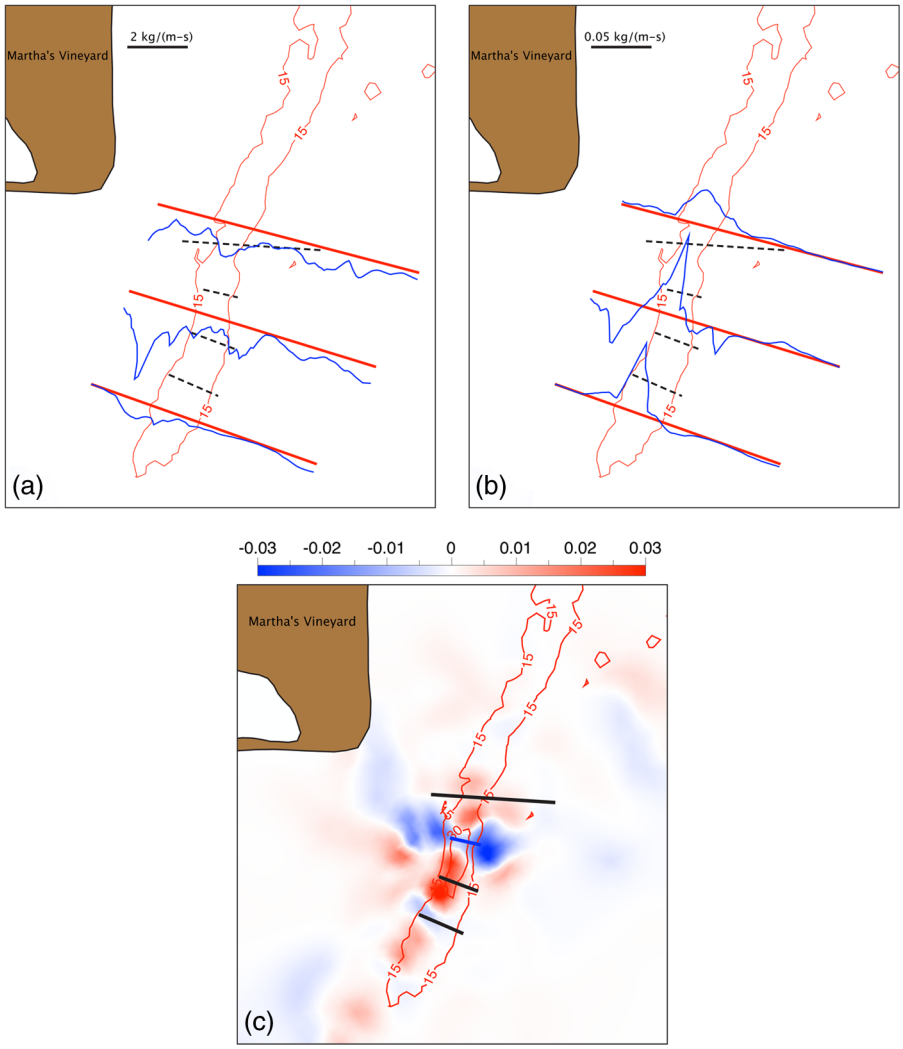

from the fluxes computed in natural conditions. Sediment flux perturbations are in the order of 0.01 kg/(m-s) corresponding to approximately 1% of the natural fluxes. During ebb, the perturbations to the transect fluxes due to augmentations in the device-influenced flow field are most significant along the central and southern transects. The largest defects in the flux (on the order of 0.05 kg/(m-s)) occur in the main channel, particularly where a flux transect is proximal to, and downstream of, the installation (e.g. the influence of a T7 installation on the middle flux transect during ebb as shown in Figure 5b). On the edge of the channel, the fluxes are enhanced due to the local increase in bed stress. The T9 installation is seen to have the smallest influence on the sediment flux, due primarily to the reduced amount of energy harvested at this site in comparison to energy extracted at T7 and T8 (Table 2). Although smaller in magnitude, flood tide sediment flux augmentations are essentially similar to ebb, with flux defects occurring in the channel and flux enhancements on the flanks.

The relative change in bed heights between turbine-modified (at T7) and natural simulations is shown in Figure 5c. This field should not be interpreted as actual accretion or erosion, rather a net accretion or erosion in the turbine-modified environment relative to evolution of the bed in natural flow conditions. In simulations with energy extraction from each transect, there is a net positive change in the bed height, which is consistent with expectations as the energy needed to erode and transport sediment is being removed from the system. In all four cases of installation along a particular transect, the spatial distribution of relative bed changes follows the basic pattern of changes in bed stress resulting from the momentum removal. There is a positive change in bed thickness in the main channel with a negative change on the flanks of the channel. Over the 30-day period, this net bed change is approximately 3 cm at the central transects (T7 and T8) and 2 cm at the northern (T6) and 0.5 cm at the southern (T9) installations. The total volume associated with the relative change in bed thickness within the domain is monotonically related to the power extracted by the devices (not shown).

Neill et al. (2009, 2012) found that 250- and 300-MW tidal stream turbine array resulting in 1 and 0.2 cm difference from natural bed level change in the period of 30 and 14 days, respectively, a relatively smaller impact compared to our estimated of a 3 cm over 30 days from a ~3-MW tidal stream turbine array in Muskeget Channel. It is difficult to compare the present results with these prior studies due to the differences in domain sizes and

modeling approaches. Neill et al. (2012) employed a single grain size and a two-dimensional Exner equation to model the evolution of the bed. Such an approach cannot account for armoring processes due to the employment of a single grain size or scour and settle lag due to the combination of suspended- and bed-load into one scalar quantity in the Exner equation.

Depth-Averaged Residual Currents

The tide-induced residual current is the result of the oscillating tidal velocity's interaction with the bottom topography (Zimmerman, 1978). In the present work, the tide-induced residual current is calculated as the mean velocity field over two spring-neap cycles. Information on residual current is important because the net transport of various material in coastal waters (e.g., sediments, larvae) is associated directly with residual currents (Tee, 1980). Alteration of the residual current, in this case due to the tidal stream turbine farm, will generate a change in the net material transport in the region.

Tidally induced, depth-averaged residual currents in Muskeget Channel and the surrounding region are shown in Figure 6a. Maximum residuals are of order 70 cm/s and occur in the vicinity of Muskeget Channel flowing southwestward. The difference between turbine-installed and natural residual current magnitude (Figure 6b) shows a velocity defect in the residual current due to turbine momentum extraction. This defect is on the order of 2 cm/s, which roughly corresponds to 3% of the natural residual current.

FIGURE 6

Tide-induced depth-averaged residual current for natural conditions (a). Difference between turbine installation-modified depth-averaged residual current magnitude (m/s) and natural conditions, following full extraction scenario (b).

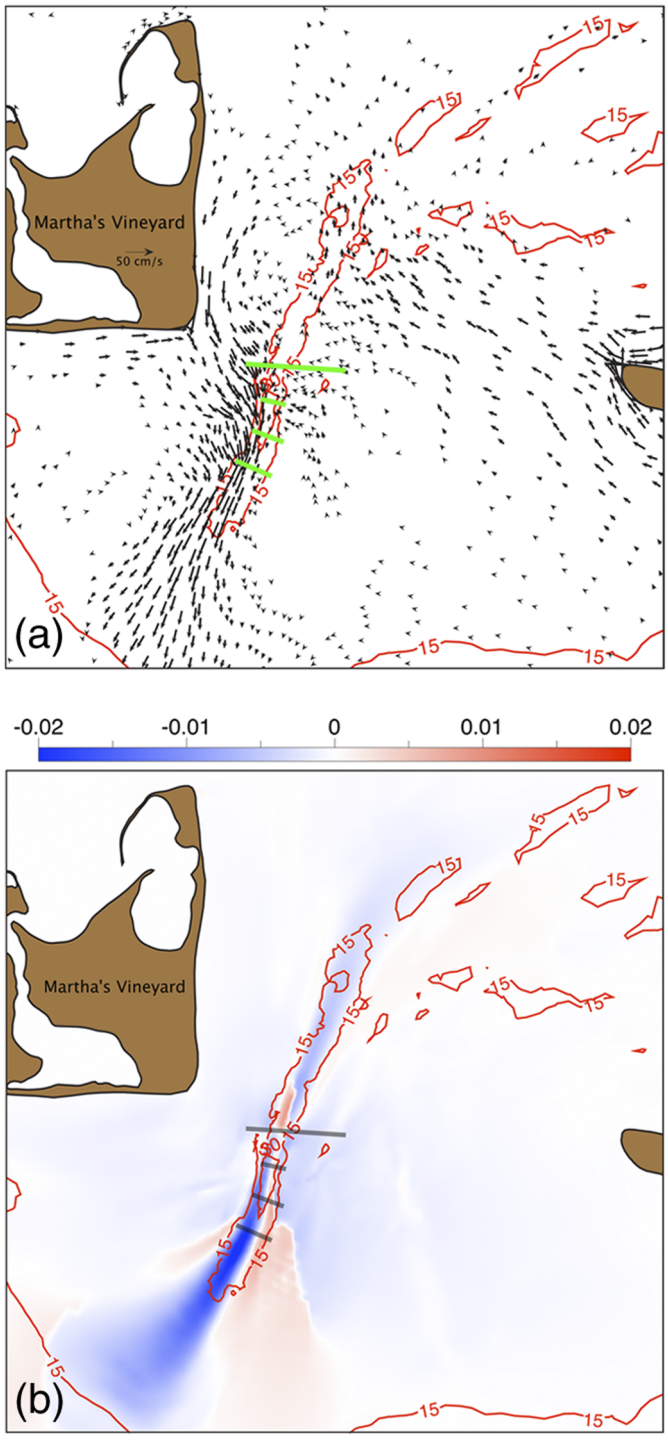

Tidal Harmonics

Observed tides in Muskeget Channel are characterized by a relatively low tidal range, on the order of 0.7 m, with a rapidly changing phase in the along-channel direction (Moody et al., 1984). Unlike other areas where strong tidal currents are due to high tidal range (e.g., Minas Basin in the Bay of Fundy), it is the rapid change of tidal phase in Muskeget Channel that drives the strong current (Chen et al., 2011).

FIGURE 7

Difference in M_2 amplitude (a) and phase (b) due to turbine installations (in m and °G, respectively) for the full extraction scenario.

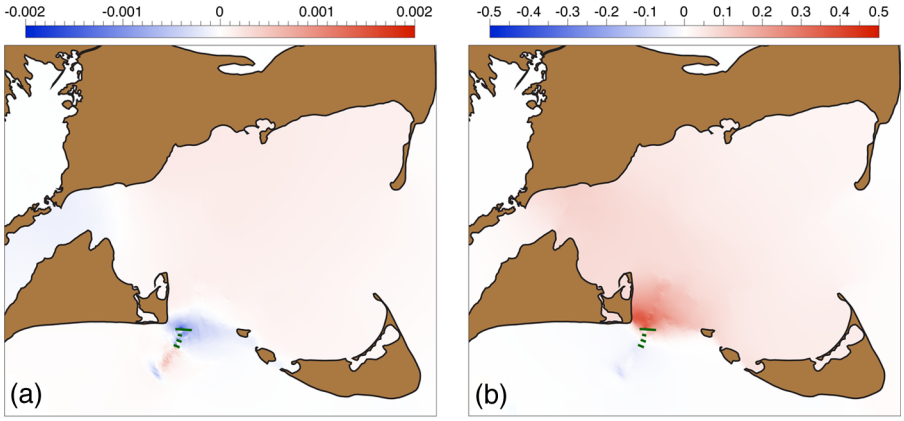

Following the full extraction scenario, the changes in the M_2 tidal amplitude and phase (Figures 7a and 7b) are on the order of less than 1 cm and 0.5° (~1 min), respectively. The largest decrease in amplitude (~0.2 cm) is observed near the MIMV section and all proposed transects. An increase in amplitude of order 0.1 cm is observed in the region located southwest of the installation. Smaller increases are seen near the central region of Nantucket Sound. As the level of the energy extraction from the channel is increased (with increasing C_p), the alteration to the M_2 harmonics changes accordingly (Table 4).

Higher-Energy Extraction

Simulation at higher levels of energy extraction was carried out to investigate the extent to which increasing the output power by enlarging the scale of the turbine farm may be achieved without negative impacts. For this experiment, we modeled the effects of the extended farms using simple artificial increases in the value of the power coefficient C_p to 0.5 (see Equation (1) and Appendix A). The impacts of extracting additional power from the channel are assessed based on examination of the resulting change in tidal residual current and tidal amplitude and phase (summarized in Table 4). This higher extraction level generated a maximum decrease of roughly 13 cm/s (19% relative to natural condition) in the residual current, 2 cm (6% relative to unperturbed amplitude) in tidal amplitude, and 10 min of tidal phase delay in the along channel direction.

Conclusions

Energy extraction experiments with turbine installations along single transects were employed to examine the near-field potential impact on hydrodynamics and sediment fluxes on each of the proposed transects of the Muskeget Channel tidal energy project (Table 5). Maximum velocity defects in the device wake during ebb are on the order of 5 cm/s. The turbine installation enhances the velocity on the flanks of the channel by approximately 2 cm/s. These perturbations to the velocity field influence the divergence of the bed stress and lead to adjustments in the bed height of up to 3 cm over a 1-month time scale. Relative to the natural power across the MIMV and MR sections (peak of ~230 MW and ~75 MW) the maximum power

TABLE 4

Summary of maximum impact following full extraction scenario (T6, T7, T8, and T9).

	C_p = 0.15		C_p = 0.5	
Property	(–)	(+)	(–)	(+)
M_2 amp (cm)	0.36	0.20	2.05	1.15
M_2 phase (°G)	0.34	0.70	1.93	4.58
Residual flow (m/s)	0.02	0.01	0.13	0.05

TABLE 5

Summary of maximum impact for the single transect installation scenario.

Property	Natural	Perturbation
Velocity	2.5 m/s	4.9 cm/s (2.5%)
Water level	35 cm	0.3 cm (0.8%)
Sediment flux	1.5 kg/(m-s)	0.01 kg/(m-s) (0.6%)
Bed level change (30 days)	33 cm	3 cm (9%)

extracted by the proposed devices at any transect (~2.7 MW at T7) represents a ratio of only 1% and 4%, respectively. Compared to natural tidal dissipation in the region bordered by the proposed transects (25.3 MW and 7.3 MW during peak ebb and flood, respectively), the output power from proposed configuration is 11% and 30% for maximum single transect (T7) and full transects installation, respectively.

The power extracted by full turbine installation of the proposed Muskeget Tidal Energy Project is a relatively small fraction of the natural power between Muskeget Island and Martha's Vineyard (the MIMV line), roughly 3% and 1% during peak ebb and flood tides, respectively. Far-field impacts on tidal harmonics and depth-averaged residual circulation were investigated for full turbine installation and found to be less than 1% change to the natural condition. A realistic tidal energy extraction scenario is likely to have little effect on water circulation as long as the extracted power remains relatively small compared with the natural power and local tidal dissipation. Higher-energy extraction affects the change in tidal harmonics (maximum 6%) and southward depth-averaged mean residual flow (maximum 19%) at Muskeget Channel. However, identification of a specific extraction limit depends on the specific metrics for impact evaluation and would require further investigation.

Appendix A. Momentum Sink Term

The accepted method for modeling tidal energy extraction is based on Linear Momentum Actuator Disc Theory (LMADT) as previously applied to wind turbine aerodynamics. See Hansen (2000) and Burton et al. (2001) for details. Failure to implement the LMADT approach correctly when formulating the additional sink terms in the model momentum equations can lead to errors in the calculated energy extraction and associated effects. An example of a correctly implemented approach is presented in Roc et al. (2013).

According to LMADT, the turbine power coefficient (C_P) and thrust coefficient (C_T) can be expressed as a function of an induction factor (a) as stated below:

$$C_P = 4a(1-a)^2 \tag{A-1}$$

$$C_T = 4a(1-a) \tag{A-2}$$

where the induction factor a is defined as

$$a = 1 - \frac{u_t}{u_0}, \tag{A-3}$$

u_0 is the free stream velocity without the presence of the disc (turbine), and u_t is the velocity at the disc (turbine). The momentum loss of the fluid due to the turbine is equal to the thrust force of the fluid on the turbine:

$$S_u = -F_T = -C_T \frac{1}{2}\rho A_t u_0^2. \tag{A-4}$$

Directly quantifying F_T based on (A-4) requires that the local undisturbed velocity (u_0) be known. Using the previous expressions above, we can express u_0 and C_T using the following:

$$u_0 = \frac{u_t}{(1-a)} \tag{A-5}$$

$$C_T = \frac{C_P}{(1-a)} \tag{A-6}$$

By substituting the above two equations into (A-4), we can express the momentum sink (thrust force) as a function of turbine power coefficient (C_P) and local velocity in the presence of turbine (u_t):

$$S_u = -F_T = -\frac{1}{2}\frac{C_P}{(1-a)^3}\rho A_t u_t^2 \tag{A-7}$$

or

$$S_u = -F_T = -\frac{1}{2}C_x \rho A_t u_t^2 \tag{A-8}$$

with the extraction coefficient (C_x) expressed as a function of the turbine power coefficient (C_P) and induction factor (a):

$$C_x = \frac{C_P}{(1-a)^3} \tag{A-9}$$

In this work, the turbine power coefficient C_P is 0.15; hence, the induction factor a is equal to 0.04 from (A-1) and the extraction coefficient C_x is 0.17.

Appendix B. Additional Turbulence Terms

The turbulence equations in FVCOM are augmented using an approach used previously in wind turbine impact studies (Réthoré et al., 2009). The following terms are computed in the MHKE module and added to the evolution equations for turbulent kinetic energy k and dissipation ε

$$S_k = \frac{C_x A_t}{2}(\beta_p u_t^3 - \beta_d u_t k) \tag{B-1}$$

$$S_\varepsilon = c_{\varepsilon 4}\frac{\varepsilon}{k}S_k \tag{B-2}$$

where S_k and S_ε are the source terms for turbulent kinetic energy and dissipation rate, respectively, and β_p, β_d, and $c_{\varepsilon 4}$ are closure coefficients for the

FIGURE B1

Velocity defect [m/s] for simulations with no inclusion of additional turbulence terms (left panel) and with inclusion of additional turbulence terms (right panel).

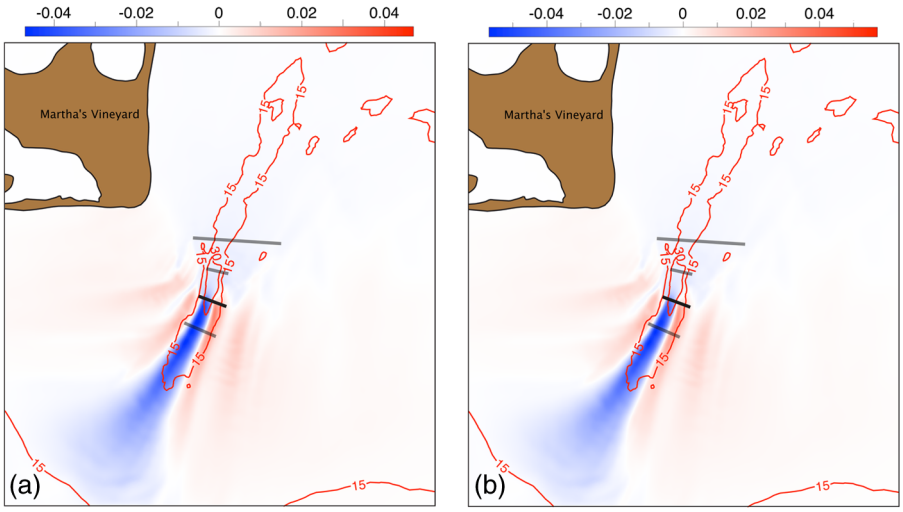

turbulent kinetic energy production and dissipation. There are indications that the values of these coefficients are specific to the flow regime at a given site. The values selected by Réthoré et al. (2009) in a study of wind turbines (β_p, β_d, and $c_{\varepsilon 4}$ are 0.05, 1.5, and 1.6, respectively) differed from those of James et al. (2010) in an evaluation of tidal turbine impact (β_p, β_d, and $c_{\varepsilon 4}$ are 1.0, 5.1, and 0.9, respectively). While reproducing the observed turbine wake from the flume study of Myers and Bahaj (2010), James et al. (2010) obtained a set of coefficients (β_p, β_d, and $c_{\varepsilon 4}$ are 1.21, 3.8, and 1.82, respectively) that differed from that of their 2010 study. When employing the values for the coefficients (β_p, β_d, and $c_{\varepsilon 4}$) used in James et al. (2010) to parameterize the additional turbulence terms in the present work, we found that there is no significant change to the wake structure downstream of the turbine (see Figure B1). This result is consistent with observations from the environmental monitoring program in Strangford Lough (UK) (Royal-Haskoning, 2011), which found no significant increase in turbulence near the bed and free surface following the installation and operation of the Marine Current Turbine SeaGen unit. Given the evidence for a lack of universal values for the coefficients and a failure to produce significant alterations to the wake structure using parameterizations from prior efforts, we chose not to include the additional turbulence terms in the present work.

Appendix C. Open Channel Validation Case

An idealized open channel flow was used to test the implementation of the subgridscale turbine extraction terms in FVCOM (Appendix A1). The open channel domain has dimensions of 10,000 m in the streamwise direction and 1,000 m in the direction normal to the flow and is discretized using a semistructured grid have orthogonal edge lengths of 100 m (Figure C1). The bathymetry has a constant value of 20 m. A free slip condition is employed along the lateral wall boundaries. The flow is driven by setting difference in free surface elevation at

FIGURE C1

Model domain (upper) and inset (lower) showing the mesh and the cells containing the turbines (indicated in blue) for the open channel validation case.

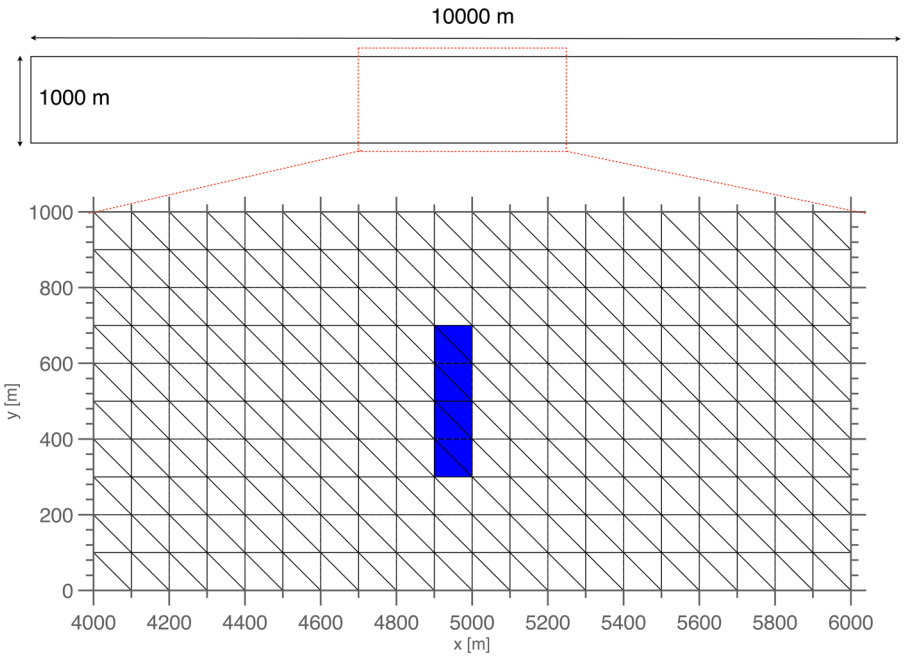

TABLE B-1

Summary of terms in the energy balance for the open channel validation case.

Power [MW]	Without Turbines	With Turbines
Inflow	413.84	347.95
Outflow	–210.53	–157.68
Bottom dissipation	–202.96	–153.91
Turbine array	–0.00	–36.07
Sum	0.35	0.28

FIGURE C2

Vertically averaged *x*-velocity (m/s) for open channel validation case with turbines.

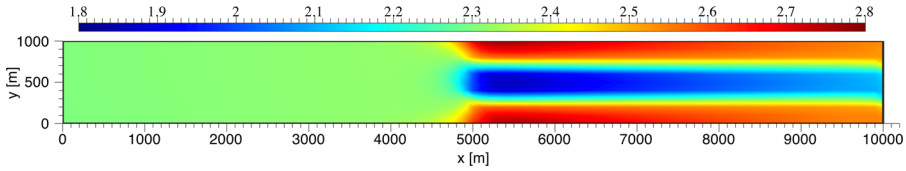

the inflow and outflow such that the net surface slope across the domain is $-5e^{-5}$ m/m, resulting in a steady depth-averaged velocity of ~2.6 m/s. Energy is extracted from eight turbines located at the center of the open channel (Figure C1) each having an extraction coefficient C_x = 1.0 and area 1,000 m^2. These numbers were selected so that the extracted energy represented a significant fraction of the available flux.

An energy balance was conducted using a control volume bordered in the streamwise by x = 1,000 m and x = 9,000 m, laterally by the walls and vertically by the bottom and free surface. The energy fluxes on the control volume surface include a source term (inflow) and three sink terms (outflow, bottom friction dissipation, and extraction by turbines):

$$E_{flux,in} = E_{flux,out} + B_{dissip} + E_{ext}. \quad \text{(C-1)}$$

The terms in the energy balance are summarized in values of power in Table B-1 below. The error in the net energy balance represents 0.08% of the total value at the inflow for cases both with and without turbines. This discrepancy derives from the need to interpolate velocity values in FVCOM from their natural location at the cell centers to the cell edges coincident with the energy control volume. The results also indicate that the presence of the turbines in the channel produces a blocking effect to the flow in the channel leading to a reduction in the farfield velocity upstream of the turbines from ~2.6 to ~2.3 m/s (Figure C2). Flow is accelerated around the edges of the array to ~2.6 m/s and flow in the wake of the array is ~2.2 m/s.

Acknowledgments

The authors would like to thank the reviewers for their valuable comments and suggestions. A. Hakim and J. Churchill were supported by the MIT Sea Grant through award NA10OAR4170066. G. Cowles was supported by the U.S. Department of Energy through award DE-EE0002656. Computations were made on the UMass Dartmouth GPU cluster, which was acquired with support from NSF award CNS-0959382 and AFOSR DURIP award FA9550-10-1-0354.

Corresponding author:

Aradea R. Hakim
Department of Fisheries Oceanography, School for Marine Science and Technology
University of Massachusetts, Dartmouth
706 S. Rodney French Boulevard, New Bedford, MA 02744
Email: ahakim@umassd.edu

References

ABPMer. 2007. Quantification of Exploitable Tidal Energy Resources in UK Waters: Main Text and Appendices. *Technical Report*. R.1349. RWE-npower. Swindon, UK. 100 pp.

Black & Veatch. 2005. Phase II UK tidal stream energy resource assessment. Technical Report 107799/D/2200/03 to the Carbon Trust. London, UK. 51 pp.

Bryden, I.G., & Couch, S.J. 2007. How much energy can be extracted from moving water with a free surface: A question of importance in the field of tidal current energy? Renew Energ. 32(11):1961-6. http://dx.doi.org/10.1016/j.renene.2006.11.006.

Burchard, H., Bolding, K., & Villarreal, M.R. 1999. GOTM—A general ocean turbulence model. Theory, applications and test cases. EUR 18745 EN. European Commission (European Union), Brussels. Belgium. 103 pp.

Burton, T., Jenkins, N., Sharpe, D., & Bossanyi, E. 2001. *Wind energy handbook*. Wiley. Chichester, UK. 617 pp.

Chen, C., Beardsley, R., & Cowles, G. 2006. An unstructured grid finite-volume coastal ocean model system. Oceanography. 19(1):78-89. http://dx.doi.org/10.5670/oceanog.2006.92.

Chen, C., Huang, H., Beardsley, R.C., Xu, Q., Limeburner, R., Cowles, G., … Lin, H. 2011. Tidal dynamics in the Gulf of Maine and New England Shelf: An application of FVCOM. J Geophys Res. 116:C12010. http://dx.doi.org/10.1029/2011JC007054.

Chen, C., Liu, H., & Beardsley, R.C. 2003. An unstructured grid, finite-volume, three-dimensional primitive equation ocean model: Application to coastal ocean and estuaries. J Atmos Oceanic Technol. 20:159-86. http://dx.doi.org/10.1175/1520-0426(2003)020<0159:AUGFVT>2.0.CO;2.

Churchill, J.H., Runge, J., & Chen, C. 2011. Processes controlling retention of spring-spawned Atlantic cod (*Gadus morhua*) in the western Gulf of Maine and their relationship to an index of recruitment success. Fish Oceanogr. 20(1):32-46. http://dx.doi.org/10.1111/j.1365-2419.2010.00563.x.

Cowles, G.W. 2008. Parallelization of the FVCOM coastal ocean model. Int J High Perform Comput Appl. 22(2):177-93. http://dx.doi.org/10.1177/1094342007083804.

Defne, Z., Haas, K.A., & Fritz, H.M. 2011. Numerical modeling of tidal currents and the effects of power extraction on estuarine hydrodynamics along the Georgia coast, USA. Renew Energ. 36(12):3461-71. http://dx.doi.org/10.1016/j.renene.2011.05.027.

Defne, Z., Haas, K.A., Fritz, H.M., Jiang, L., French, S.P., Shi, X., … Stewart, K.M. 2012. National geodatabase of tidal stream power resource in USA. Renew Sust Energ Rev. 16(5):3326-38. http://dx.doi.org/10.1016/j.rser.2012.02.061.

Denny, J.F., Danforth, W.W., & Signell, R.P. 2012. Bathymetric data collected within Muskeget Channel, Massachusetts: U.S. Geological Survey Open-File Report 2012-1258 (accessed from http://pubs.er.usgs.gov/publication/ofr121258).

de Vriend, H.J., Capobianco, M., Chesher, T., De Swart, H.D., Latteux, B., & Stive, M.J.F. 1993. Approaches to long-term modelling of coastal morphology: a review. Coast Eng. 21(1):225-69. http://dx.doi.org/10.1016/0378-3839(93)90051-9.

Eakins, B.W., Taylor, L.A., Carignan, K.S., Warnken, R.R., Lim, E., & Medley, P.R. 2009. Digital Elevation Model of Nantucket, Massachusetts: Procedures, Data Sources and Analysis, NOAA Technical Memorandum NESDIS NGDC-26. Dept. of Commerce. Boulder, CO. 29 pp.

Ganju, N.K., & Sherwood, C.R. 2010. Effect of roughness formulation on the performance of a coupled wave, hydrodynamic, and sediment transport model. Ocean Modelling. 33(3):299-313.

Hagerman, G., & Bedard, R. 2006. Massachusetts tidal in-stream energy conversion (TISEC): Survey and characterization of potential project sites. *Technical report*, TP-003-MA. EPRI, Washington, DC. 56 pp.

Hakim, A., Cowles, G., & Churchill, J. (in preparation). A high resolution numerical model for tidal energy resource assessment in Massachusetts.

Hansen, M.O. 2000. *Aerodynamics of Wind Turbines: Rotors, Loads and Structure*. James & James. London, UK. 144 pp.

Howes, B., Samimy, R., Schlezinger, D., Bartlett, M., & Benson, J. 2009. Marine renewable energy survey of Muskeget Channel. *Technical Report Prepared for the Massachusetts Technology Collaborative*, UMass Dartmouth. New Bedford, MA. 88 pp.

Huret, M., Runge, J., Chen, C., Cowles, G., Xu, Q., & Pringle, J. 2007. Dispersal modeling of fish early life stages: sensitivity with application to Atlantic cod in the western Gulf of Maine. Mar Ecol Prog Ser. 347:261-74. http://dx.doi.org/10.3354/meps06983.

James, S.C., Seetho, E., Jones, C., & Roberts, J. 2010. Simulating environmental changes due to marine hydrokinetic energy installations. OCEANS 2010:1-10. IEEE.

James, S.C., Barco, J., Johnson, E., Roberts, J.D., & Lefantzi, S. 2011. Verifying marine-hydro-kinetic energy generation simulations using SNL-EFDC. OCEANS 2011:1-9. IEEE.

Jameson, A. 1995. Analysis and design of numerical schemes for gas dynamics 1, artificial diffusion, upwind biasing, limiters and their effect on multigrid convergence. Int J Comp Fluid Dyn. 4:171-218. http://dx.doi.org/10.1080/10618569508904524.

Meyer-Peter, E., & Müller, R. 1948. Formulas for bed-load transport. *Proceedings of the 2nd Meeting of International Association for Hydraulic Structures Research, Stockholm, Sweden*. Int. Assoc. for Hydraulic Res., Madrid. pp. 39–64.

Myers, L.E., & Bahaj, A.S. 2010. Experimental analysis of the flow field around horizontal axis tidal turbines by use of scale mesh disk rotor simulators. Ocean Eng. 37(2):218-27. http://dx.doi.org/10.1016/j.oceaneng.2009.11.004.

McEntee, J. 2010. Preliminary tidal energy assessment for Muskeget Channel. *Technical Report Prepared for HMMH for Town of Edgartown*, Ocean Renewable Power Company. Portland, ME. 12 pp.

Moody, J.A., Butman, B., Brown, W., Daifuku, P., Irish, J., Mayer, D., … Wright, W. 1984. Atlas of tidal elevation and current observations on the northeast American continental shelf and slope. U.S. Geological Survey Bulletin 1611. Alexandria, VA. 122 pp.

National Research Council. 2013. An Evaluation of the U.S. Department of Energy's Marine and Hydrokinetic Resource Assessments. *National Academy of Science*. Washington, DC. 154 pp.

Neill, S.P., Jordan, J.R., & Couch, S.J. 2012. Impact of tidal energy converter (TEC) arrays on the dynamics of headland sand banks. Renew Energ. 37(1):387-97. http://dx.doi.org/10.1016/j.renene.2011.07.003.

Neill, S.P., Litt, E.J., Couch, S.J., & Davies, A.G. 2009. The impact of tidal stream turbines on large-scale sediment dynamics. Renew Energ. 34(12):2803-12. http://dx.doi.org/10.1016/j.renene.2009.06.015.

Polagye, B., Kawase, M., & Malte, P. 2009. In-stream tidal energy potential of Puget Sound, Washington. Proc Inst Mech Eng:

A. J Power Energy. 223(5):571-87. http://dx.doi.org/10.1243/09576509JPE748.

Poppe, L.J., & Polloni, C.F. 2000. USGS East-coast sediment analysis: Procedures, database, and georeferenced displays. *Technical Report Open-File Report 00-358*. U.S. Geological Survey (accessed from http://pubs.er.usgs.gov/publication/ofr00358).

Ralston, D.K., Geyer, W.R., Lerczak, J.A., & Scully, M. 2010. Turbulent mixing in a strongly forced salt wedge estuary. J Geophys Res. 115:C12024.

Réthoré, P.E., Sorensen, N.N., & Bechmann, A. 2009. CFD model of wind turbine wake in atmospheric turbulence using body forces. Technical report, IEA Offshore Wake Workshop. Risø, Denmark. 19 pp.

Roc, T., Conley, D.C., & Greaves, D. 2013. Methodology for tidal turbine representation in ocean circulation model. Renew Energ. 51:448-64. http://dx.doi.org/10.1016/j.renene.2012.09.039.

Roworth, E., & Signell, R. 1998. Construction of digital bathymetry for the Gulf of Maine. *Technical Report Open-File Report 98-801*, U.S. Geological Survey (accessed from http://pubs.er.usgs.gov/publication/ofr98801).

Royal-Haskoning. 2011. SeaGen Environmental Monitoring Programme. *Marine Current Turbine*: 9S8562/R/303719/Edin. Edinburgh, UK. 77 pp.

Shapiro, G. 2011. Effect of tidal stream power generation on the region-wide circulation in a shallow sea. Ocean Sci. 7:165-74. http://dx.doi.org/10.5194/os-7-165-2011.

Simpson, J.H., & Hunter, J. R. 1974. Fronts in the Irish Sea. Nature. 250:404-6. http://dx.doi.org/10.1038/250404a0.

Tee, K.T. 1980. The structure of three-dimensional tide-induced current. Part II: Residual currents. J Phys Oceanogr. 10(12): 2035-57. http://dx.doi.org/10.1175/1520-0485(1980)010<2035:TSOTDT>2.0.CO;2.

Walkington, I., & Burrows, R. 2009. Modelling tidal stream power potential. Appl Ocean Res. 31(4):239-45. http://dx.doi.org/10.1016/j.apor.2009.10.007.

Warner, J.C., Sherwood, C.R., Signell, R.P., Harris, C.K., & Arango, H.G. 2008. Development of a three-dimensional, regional, coupled wave, current, and sediment-transport model. Comput Geosci. 34:1284-306. http://dx.doi.org/10.1016/j.cageo.2008.02.012.

Weisberg, R.H., & Zheng, L. 2006a. Hurricane storm surge simulations for Tampa Bay. Estuar Coasts. 29(6):899-913.

Weisberg, R.H., & Zheng, L. 2006b. A simulation of the Hurricane Charley storm surge and its breach of North Captiva Island. Florida Scientist. 69:152.

Work, P.A., Haas, K.A., Defne, Z., & Gay, T. 2013. Tidal stream energy site assessment via three-dimensional model and measurements. Appl Energ. 102:510. http://dx.doi.org/10.1016/j.apenergy.2012.08.040.

Yang, Z., Wang, T., & Copping, A.E. 2013. Modeling tidal stream energy extraction and its effects on transport processes in a tidal channel and bay system using a three-dimensional coastal ocean model. Renew Energ. 50:605-13. http://dx.doi.org/10.1016/j.renene.2012.07.024.

Zimmerman, J. 1978. Topographic generation of residual circulation by oscillatory (tidal) currents. Geophys Astrophys Fluid Dyn. 11(1):35-47. http://dx.doi.org/10.1080/03091927808242650.